Key Engineering Materials
ISSN: 1662-9795, Vol. 926, pp 147-158
doi:10.4028/p-g7ip54

Submitted: 2021-12-07
Accepted: 2022-02-18
Online: 2022-07-22

Selective Laser Melting of Ti-6Al-4V Lattices: Case Study on a Spinal Cage Prosthesis

Francesco Cantaboni[1,a*], Paola Ginestra[1,b], Marialaura Tocci[1,c], Elisabetta Ceretti[1,d], Giulia De Sio[1,e], Xue Cao[2,f], Luke N. Carter[2,g], Victor M. Villapún[2,h], Morgan Lowther[2,i], Sophie Louth[2,l] and Sophie C. Cox[2,m]

[1]Department of Mechanical and Industrial Engineering, University of Brescia, V. Branze 38, 25123 Brescia, Italy

[2]School of Chemical Engineering, College of Engineering and Physical Sciences, University of Birmingham, Edgbaston, UK. B15 2TT

[a]f.cantaboni@unibs.it, [b]paola.ginestra@unibs.it, [c]marialaura.tocci@unibs.it, [d]elisabetta.ceretti@unibs.it, [e]g.desio@studenti.unibs.it, [f]xxc867@student.bham.ac.uk, [g]l.n.carter@bham.ac.uk, [h]v.m.villapun@bham.ac.uk, [i]MXL782@student.bham.ac.uk, [l]SEL713@student.bham.ac.uk, [m]S.C.Cox@bham.ac.uk

*Corresponding author

Keywords: Powder bed fusion, Lattice structure, Porosity, Case study.

Abstract. Biomedical prostheses are artificial devices suitable for the replacement of missing or inefficient parts of the body, implanted to reduce the anatomical or functional deficiency, and sometimes also applied for aesthetic purposes.
Despite this type of medical devices represents today a very innovative sector from the medical and engineering point of view, some issues, inherent to the interaction between human body and the external hosts must be considered. It is important that the weight and porosity of the prosthesis respect the patient's physiological equilibrium which permit an appropriate osseointegration where needed.
A typical solution is a lattice structure, which can be manufactured by Additive Manufacturing techniques which, as known, permit to build complex geometries in comparison with other processing routes.
Lattice structure are typically characterized by both stiffness and strength significantly lower than the full part of the structure. Generally, for this reason, the lattices are applied to the low-stress areas, leaving a portion of solid sufficient to transmit the loads involved, or in such a way to guarantee the desired flexibility of the part-itself. During the design of lattices some limitations regarding their printability must be considered, such as the minimum printable dimension and the necessary support parts.
A Design of Experiment analysis was conducted to identify the optimal parameters to manufacture a spinal cage with negligible porosity via laser powder bed fusion using Ti6Al4V alloy.

1. Introduction

Research on orthopedic implants is in constant growth since the increase in average life spanned globally. In particular, an increasing sport life style of older people required a solution to maintain an optimal mechanical function of the human body at an advanced age [1,2]. 3D printing is a perfect technology to produce customized devices due to its flexibility. In fact, products are built layer by layer, ensuring a high freedom of design [3]. For the metallic materials, Powder Bed Fusion (PBF) technologies can be used, classified in two sub-categories, according to the source of energy used: laser or electron beam. Both these technologies are based on the same working principle: the selective melting of a powder bed followed by a rapid solidification [4]. Various alloys can be processed using Laser Powder Bed Fusion (L-PBF), such as stainless steel, Al, Cu, Co and Ti alloy. Ti-6Al-4V alloy, which is most used for the fabrication of orthopedic prostheses, is of particular interest for its mechanical properties [5,6].

Thanks to this innovative technology, it is possible to produce components with very complex geometries and porous structures, such as lattice. These parts can be integrated with a prosthesis in such a way to promote osteointegration without the application of bone cement, needed to fix the bone to the external host [7,8].
L-PBF is controlled by several parameters, and the physical phenomena taking place are particularly complex. In addition, during the process, various defects can form in the product which directly affect the final density of the structure, such as gas porosity, lack of fusion porosities, and oxide layers. Several studies focused on the improvement of quality of AM components, and a design of experiment analysis is often needed to identify the proper printing parameters to have negligible defects [4].
Due to the possibility to build complex geometry we decided to print a customized prosthesis by L-PBF composed by a full dense part, where the load is focused, and a lattice part where the load is absent. Thanks to statistically relevant tests, it is possible to optimize the printing parameters to achieve the best results.

2. Materials and Methods

Fabrication and methodology

In this work, Ti-6Al-4V powder was chosen to produce cubic lattice structures. The dimensions of the samples were 20 mm^3, characterized by diamond unit cells of 1 mm^3, with the strut dimension set to 250 μm, because it is a suitable diameter to have a reasonable relative density of the lattice.
The RenAM 500M (Renishaw, UK) was used to print the lattices, designed using nTopology Element (nTopology Inc., 1.25.0). The main printing parameters are laser power and scanning speed, which were varied respectively in a range of values of 50W – 150W and 750mm/s – 2250mm/s. The hatching space was set to 45 μm. Once printed, the samples were detached from the substrate using Wire EDM (electro-discharge machining, CUT 20, Switzerland) and then cold mounted in acrylic resin. Furthermore, the samples were grinded on MD-Piano 220, with 1200 and 4000 grinding discs and subsequently polished with MD-Piano Chem on both flat sides, to obtain a mirror finish surface. The samples were observed using a scanning electron microscope (SEM, Hitachi TM3000, Japan), to acquire images of the strut sections. In principle, a preliminary study was conducted, where twenty images (Figure 1) were analyzed per sample and the size of the struts and the pores was then measured using ImageJ software. Due to the building angle, the strut cross-section appeared as an ellipse. It was assumed that the minor axis of an ellipse fitted to the area would provide the strut diameter. Thus, the "fit ellipse" function was utilized for the area quantification. This allowed to classify the struts in three categories, as shown in Figure 1. This analysis allowed to obtain the best printing parameters, which combined negligible porosity.

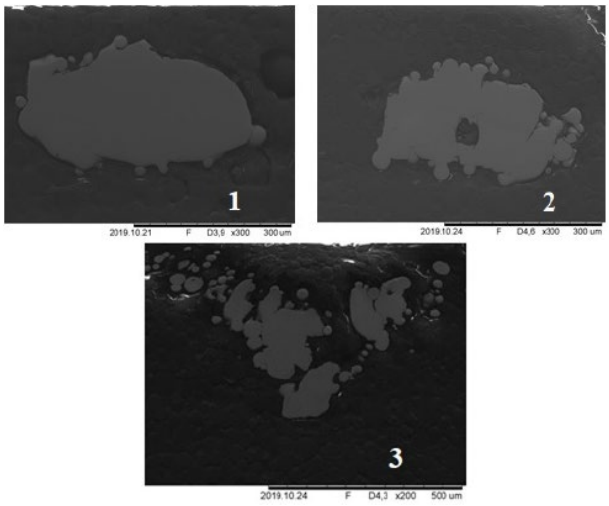

Figure 1:SEM image Strut with: 1- solid core and 2- hole in the center (porosity), 3- Damaged strut.

Furthermore, a design of experiment analysis was carried out, where the struts accuracy and the porosity level were investigated to define the best parameters to print the case study.

Preliminary study

After the analysis of the images, the porosity percentage was calculated as the ratio of the total area of the porous section and the total area of the struts present in the lattice. A porosity level of 0.25% was set as the reasonable limit for each lattice section. Thus, if the lattice section exhibited a porosity value above that limit, the sample was classified as porous. On the other hand, if the porosity value was below that limit, it was considered as non-porous. This study was carried out to validate the manufacturing process and to understand the influence of process parameters on the porosity level, with the final aim of identifying the optimal values of power and scan speed of the laser to minimize porosity.

Design of Experiment

A further study, related to the previous one, will be discussed in this section, in order to investigate the optimal parameters to print the struts with optimal size accuracy.
It was necessary to reduce the parameters studied previously to get as close as possible the value of 250 μm.
Power and scan speed were varied on three levels respectively, as represented in Table 1.

Table 1: DOE data.

Factors	Levels	Values
Power	3	50 W 100 W 150 W
Scan speed	3	750 mm/s 1125 mm/s 1500 mm/s

For each of these nine combinations, three repetitions were performed: in total, therefore, 27 specimens were printed.

3. Results

Preliminary study results

The name of the samples was defined by two numbers, where the first one was referred to the power value, while the second one corresponded to the scanning speed. The results obtained were divided in 50 W, 70 W and 90 W as shown respectively in Table 2, Table 3 and Table 4.

Table 2: Measured diameter and porosity at 50W.

Sample	Diameter [µm]	Porosity %
50-750	204±20	0,57%
50-1000	200±16	0,77%
50-1250	196±27	2,51%

Table 3: Measured diameter and porosity at 70W.

Sample	Diameter [µm]	Porosity %
70-1000	219±12	0,07%
70-1250	202±12	0,14%
70-1500	197±12	1,43%
70-1750	180±18	1,18%

Table 4: Measured diameter and porosity at 90W.

Sample	Diameter [µm]	Porosity %
90-1000	247±24	0,00%
90-1250	217±11	0,01%
90-1500	202±11	0,14%
90-1750	204±12	0,09%
90-2250	194±20	1,65%

For each considered value of laser power, different levels of scanning speed were used, to understand which was the most influencing process parameter. Firstly, a power of 50 W, was combined with three values of speed as shown in Table 2. It can be noted an increasing trend of porosity [9]. Due to these results, it was decided to do a deeper investigation with a higher value of power, but this time with higher values of velocity too, to understand what was changed in that area, as shown in Table 3. Also here, an increasing trend was identified, but which stabilized above 1500 mm/s. Therefore, it was decided to increase the power value to 90 W, and keep the four speed values used before with one more value of 2250 mm/s, to check the trend above 1500 mm/s. As shown in Table 4, the same trend as before was found, but this time with a lower value of porosity, except for 2250 mm/s, where the porosity was drastically increased for the high value of speed. Probably this speed value was too high for 90 W and it resulted in the formation of more porosities [9].
Once defined the trend with the first three values of power, other two values of power were tested, as shown in Table 5 and Table 6.

Table 5: Measured diameter and porosity at 105W.

Sample	Diameter [µm]	Porosity %
105-1250	234±13	0,05%
105-1500	217±12	0,08%
105-1750	230±24	0,09%
105-2250	201±15	2,75%

Table 6: Measured diameter and porosity at 150W.

Sample	Diameter [µm]	Porosity %
150-2250a	219±11	0,11%
150-2250b	215±9	0,12%

The lowest speed value used with 90 W was discharged because 1000 mm/s is too low for these higher power values. Also here, an increasing trend of porosity was seen, but once again, the speed of 2250 mm/s has resulted in a really high porosity.
Finally, to understand what happened with a speed of 2250 mm/s, the power value was increased to 150 W and tested only with that speed value, but this time with one repetition. As shown in Table 6, the porosity became negligible thanks to the combination of high scan speed and a higher power value. This speed value was too high to build the samples, because it required very high value of power.
The results of the porosity percentage were reported in Figure 2 which indicates that 60% of the lattice produced for this preliminary study presented full core struts.
In particular, samples showed negligible porosity when the power value was in a range between 90 W and 105 W and the speed was between 1000 mm/s and 1750 mm/s.

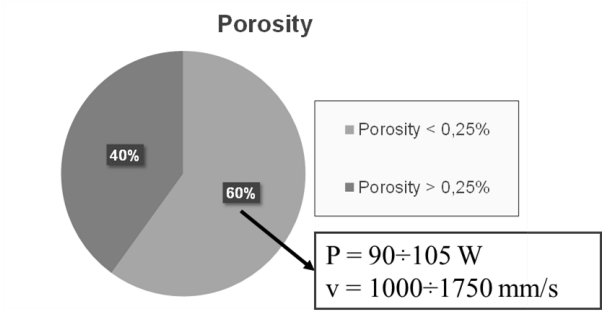

Figure 2: Porosity percentage evaluation.

For a better understanding, experimental tests were carried out to focus the study on a smaller window of parameters.

DOE results

In this second step the diameter of the struts was evaluated, because the porosity has been already investigated during the preliminary study.
27 lattices were built and analyzed under SEM, which was useful to verify the process stability to carry out the DOE study.
The poor surface finishing of products manufactured using L-PBF is a well-known limitation of this technology [9,10]. As visible in Figure 3, the surface of the struts is very irregular due to the presence of several unmelted particles, partially melted particles, or spatters. This makes difficult to properly assess the size of the struts.

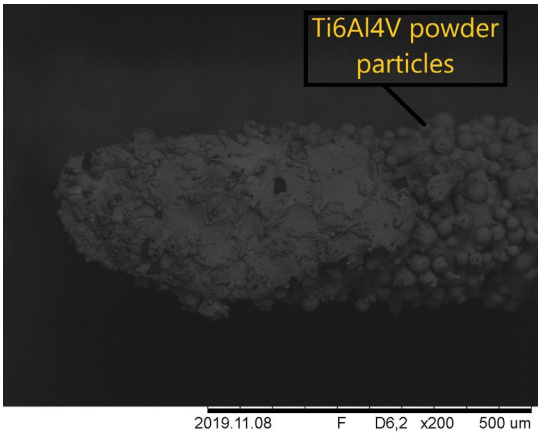

Figure 3: Image 25x magnification lattice structure with surface defects.

In the present study, it was decided to measure the struts diameter including the defects (unmelted powders, partially melted powders, spatters) eventually present, as shown in Figure 4.

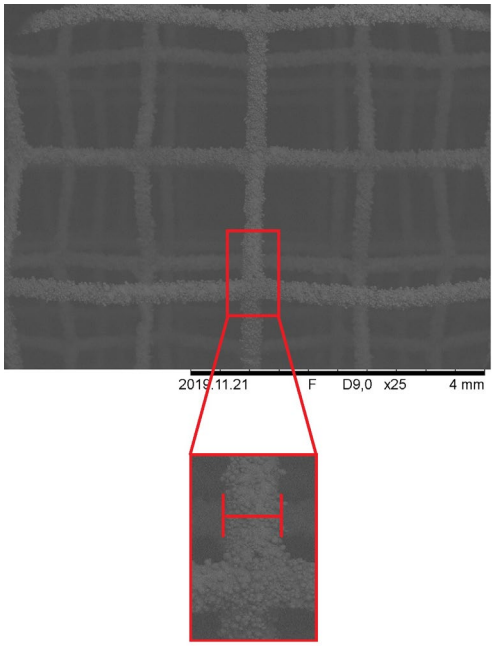

Figure 4: Image 200x magnification lattice structure and strut diameter calculation.

The obtained results are reported in Table 7. The variability of the measurements is shown in Figure 5.

Table 7: Diameter size of As built samples.

Sample	Diameter [µm]
50-750	317±22
100-750	367±59
150-750	376±50
50-1125	312±23
100-1125	327±23
150-1125	381±53
50-1500	*failed*
100-1500	348±109
150-1500	336±22

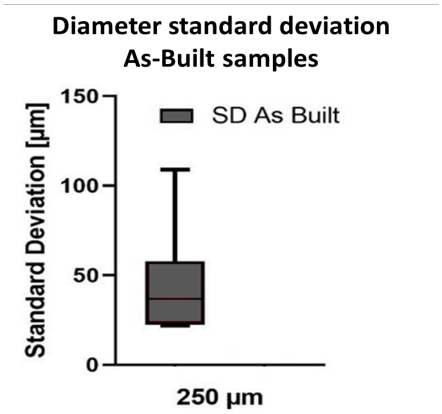

Figure 5: Diameter standard deviation of as built samples.

It can be noticed that in Table 7 the standard deviation for the sample built with 100 W and 1500 mm/s is extremely high, this could be explained by the presence of un-melted powder on the structure which can affect the size of the strut diameter, such as for the other samples. In addition, with a scanning speed of 1500 mm/s, and a power of 50 W and 100 W, the struts are not properly built [9].
Once the values of the diameters and relative standard deviations of the as-built specimens were collected, samples were cold mounted, grinded and polished to study the cross section. The diameter of the struts was measured using the same procedure applied before.
The results are reported in Table 8. In this way between these two measurement methods the differences were marked. The standard deviation (Figure 6), as expected, is significantly lower than in the previous study. This is because the dimensional measurement of the cross section of the struts is more accurate.
The standard deviation of these latter measurements was represented graphically in Figure 6 to highlight the low variability of the output diameter. It was immediately appreciable that the standard deviation related to this kind of specimens was more uniform, and it was decided to proceed with a DOE analysis focused on them.

Table 8: Diameter size of struts section.

Sample	**Diameter [µm]**
50-750	205±21
100-750	254±8
150-750	307±8
50-1125	195±9
100-1125	232±14
150-1125	291±34
50-1500	*failed*
100-1500	221±14
150-1500	246±12

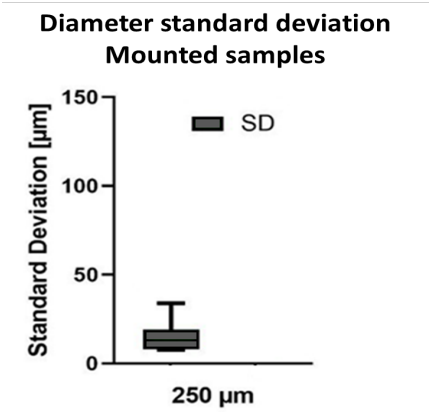

Figure 6: Diameter standard deviation of struts section.

Once the DOE study was performed, the 3D scatterplot and the contour plot respectively showed in Figure 7 and Figure 8, were plotted to understand the trend of the optimal parameters.
In the scatterplot there are two bands of points, considering the following main restrictions:

$$|D - D_0| > 10\mu m, Red$$
$$|D - D_0| < 10\mu m, Green$$

where D represents the average diameter calculated in DOE analysis, while D0 represents the nominal value of 250 µm that is aimed to be obtained. This distribution showed two couples of points in the optimum range at the ends of the graph with power respectively of 100 W and 150 W and speed of 750 mm/s and 1500 mm/s. In addition, in the center of the scatterplot a single optimum point appears, with a power of 100 W and scan speed of 1150 mm/s, and in one of the ends of the graph another single point in the optimum range is identified, with process parameters of 150 W and 1150 mm/s, but these two values were in the limit of range, because the difference between D and D0 was really close to 10 µm.
In Figure 8, it was plotted the accuracy by calculating a maximum deviation of 10 µm given by D-D0 in order to highlight the different areas of struts size.
From the graph shown in Figure 8 an optimal central band can be noticed: in particular, at the ends of it, there was a greater precision because the distribution of the optimum points had a greater concentration. It was important to underline that the general optimum trend follows an increasing behavior. In fact, the highest precision has been achieved when power and scan speed increase proportionally. Moreover, it was possible to work according to the limits of the printer (under 2000 mm/s of scan speed) varying the scan speed between 750 mm/s and 1500 mm/s, while it was always possible to get the optimal strut diameter just varying the power value between 75 W and 150 W. This was a confirmation of the greater influence of power on the results in relation to the scan speed.

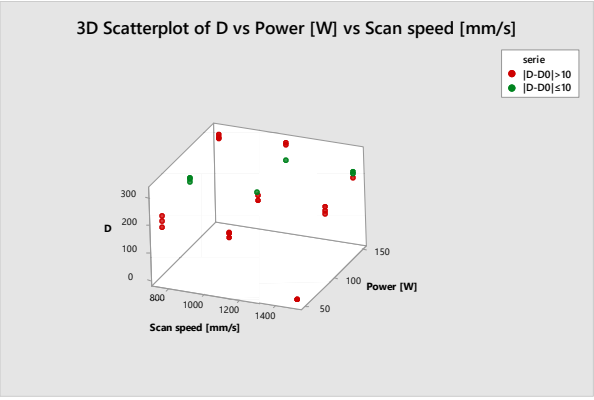

Figure 7: 3D Scatterplot of D vs Power vs Scan speed.

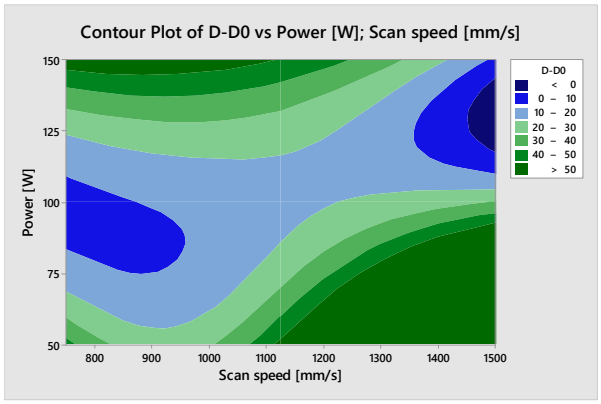

Figure 8: Contour plot of D-D0 vs Power vs Scan speed.

Moreover, the porosity and the accuracy were put in comparison by plotting them into two different graphs, as shown in Figure 9 and Figure 10.

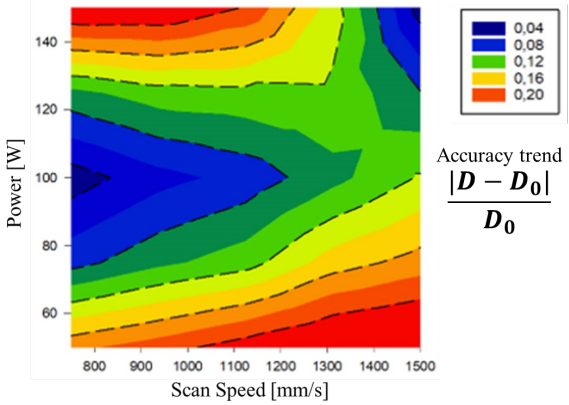

Figure 9: Contour plot of accuracy.

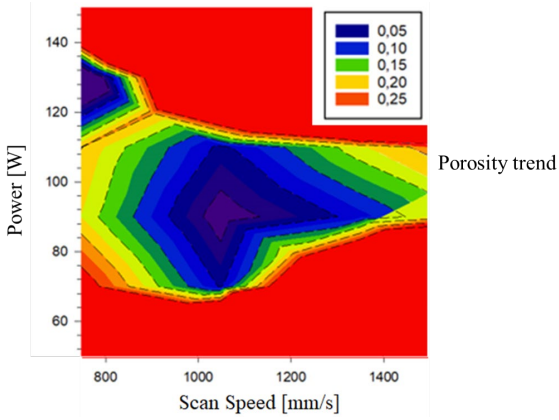

Figure 10: Contour plot of porosity.

The limit for the accuracy was set at 0,04 as a reference since it is the ratio between 10 μm and 250 μm and thus it represented the minimum acceptable deviation from the aimed diameter result.
From the two graphs, it can be noticed that, although two areas of optimum have been obtained, only one of these has a porosity lower than 0,25% (as discussed in the previous chapter). The power value of 100 W was identified as optimal for its good combination of low porosity and good accuracy, which is possible to see in Figure 9 and Figure 10. The scan speed value of 750 mm/s was identified as most adequate for the same reasons, and also because with a lower speed level it is easier to control the printing process.

4. Case Study – Spinal Cage

Design, accuracy, and porosity analysis

An application case of spinal implants, which are a clear example of implant where a lattice structure may be applied, was studied. The cage CAD file was designed as shown in Figure 11.

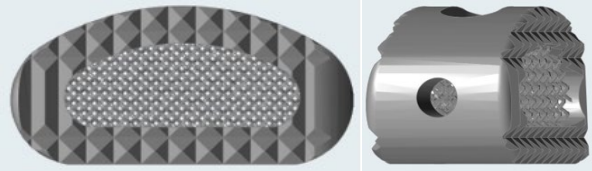

Figure 11: Designed 3D spinal cage.

The considerable advantage of using a lattice is that implants with microrough surface topographies and porosity have been shown to promote direct bone on growth, in growth and vascularization [1]. The aim was to extend the study of a lattice structure to a case of actual application where it can be integrated, evaluating the feasibility of the study from a practical and concrete point of view.
The purpose was to focus on the analysis of the porosity and the precision of the printed strut diameter. However, the case study was focused on obtaining further confirmation of the results obtained previously and it was assessed how much effectively a change in the three-dimensional shape affected the previous conclusions. The full part was printed using power of 200 W and a scan speed of 1500 mm/s to have a solid structure, while the reticulated part had as input the pair of optimal parameters previously detected, i.e. power of 100 W and scan speed of 750 mm/s. The size of the unit cell was changed to verify if the optimal parameters were still valid modifying the degree of structural porosity of the lattice.
The print was started forcing the process limits of the machine in morphological terms, since the strut and the cell were dimensionally comparable. In this case, in the preliminary phase a deviation from the optimal diameter of 10 μm was set.
An average diameter of the struts of 224±15 μm with a porosity lower than 0.25%, was recorded. Considering the very small cell dimensions (2x2x2 mm^3), the results achieved could be considered optimal. In fact, the strut did not have the opportunity to expand as much as before due to the geometric constraints.
Regarding the evaluation of porosity, some demonstrative images are shown in Figure 12.

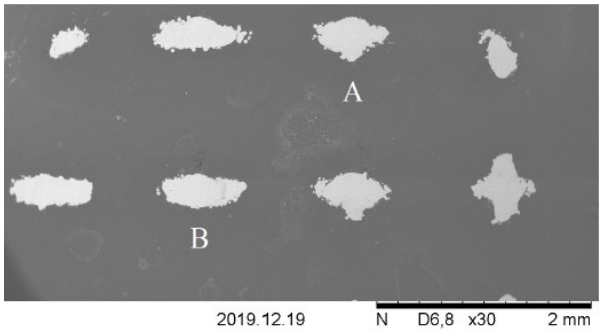

Figure 12: SEM demonstrative image of the struts.

Thanks to the set process parameters, a porosity of almost zero was recorded, as can be seen from Figure 13.

Microstructural characterization

To have a better evaluation of reliability and efficiency of the process, the microstructure of the product was also analyzed, which is strongly influenced by the process parameters used. In fact, the typical high cooling rates of the process influence the phase transformations during the solidification by determining specific microstructural features.
A cross section of the produced spinal cage was observed after polishing to mirror finishing and etching with Kroll's reagent to identify the main microstructural features.

Figure 14 shows the alloy microstructure. It is composed by a fine lamellar (Widmänstatten) α+β microstructure. This microstructure is consistent with the combination of high scanning speed and high thermal gradient with fast cooling rate typical of the process and it is widely reported in the literature for the same alloys processed with similar parameters [1], indicating the stability of the process, not only in terms of porosity level and geometrical accuracy.

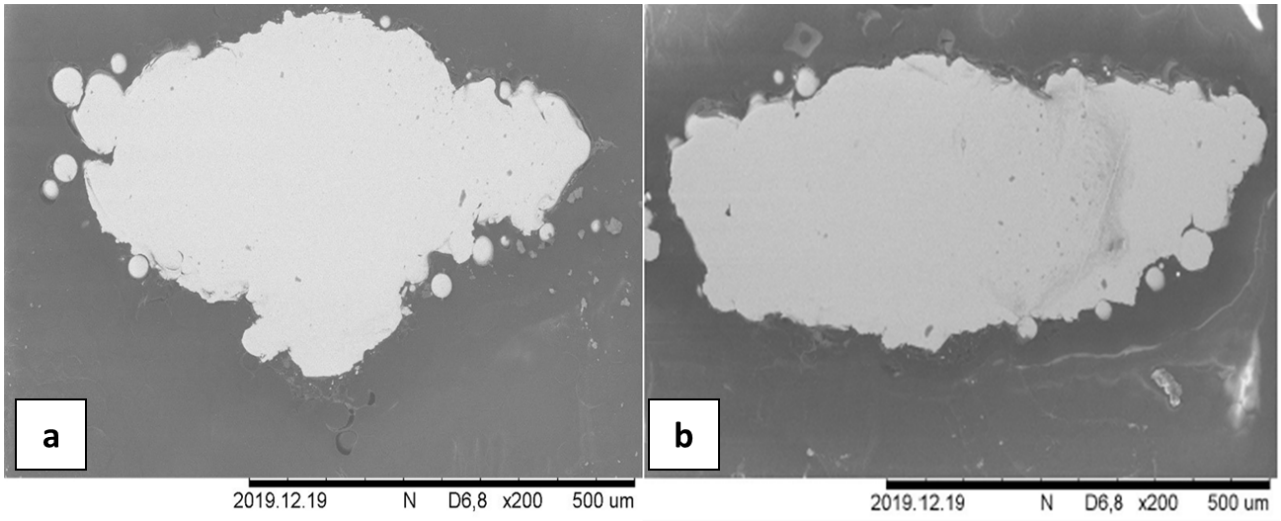

Figure 13: Struts detail A and B of Figure 12.

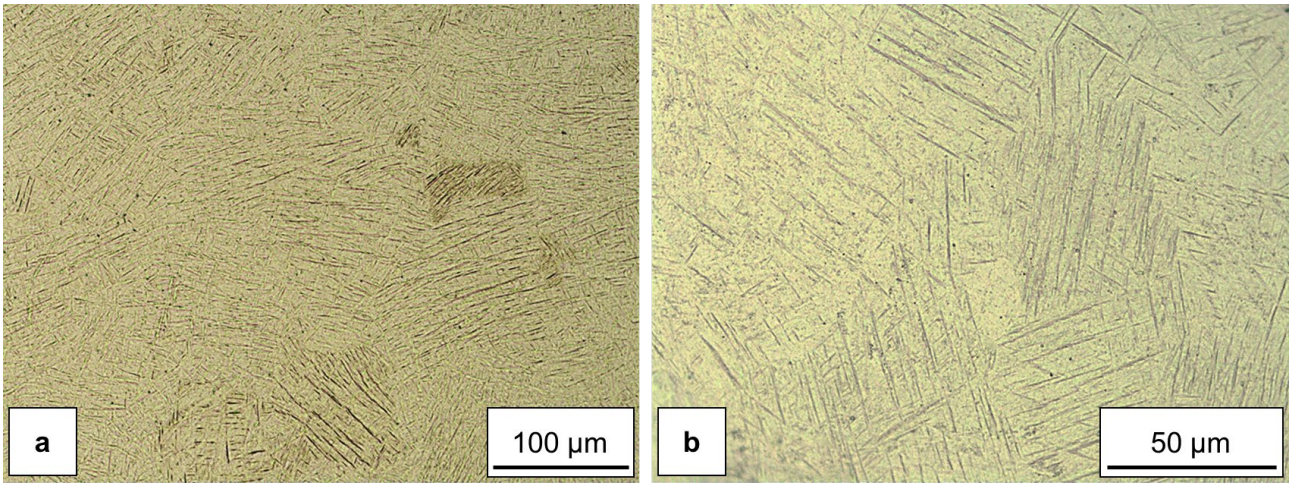

Figure 14: a) Ti-6Al-4V alloy microstructure and b) microstructure at higher magnification.

5. Conclusions

The main aim of this work was to analyze the porosity and the reliability of the results achieved of lattice structure of Ti-6V-4Al alloy manufactured by L-PBF. The process parameters were varied to reach negligible porosity and designed diameter of the struts, finally used to produce a spinal cage case study.

The first analyses were focused on narrowing the window of parameters, in order to be able to estimate in a fast way the optimal parameters necessary to achieve the diameter corresponding to 250 µm. It was necessary to change the scan speed and the power of laser to understand which one of them was more influent to reach the stability of the process. In particular, the preliminary study was carried out to the evolution of porosity varying these two parameters. Moreover, due to the DOE analysis, the highest precision has been achieved. Laser scan speed of 750 mm/s and laser power of 100W allowed to achieve a good combination of low porosity and good accuracy. In fact, the designed strut diameter, needed to produce the case study, was manufactured.

Finally, the porosity and the struts diameter of the spinal cage were measured and the Ti-6V-4Al microstructure was investigated. It was found the designed diameter size with negligible porosity and the typical microstructure, indicating the stability of the process.

References

[1] T. Majumdar, N. Eisenstein, J. E. Frith, S. C. Cox, and N. Birbilis, "Additive Manufacturing of Titanium Alloys for Orthopedic Applications: A Materials Science Viewpoint," *Adv. Eng. Mater.*, vol. 20, no. 9, 2018, doi: 10.1002/adem.201800172.

[2] G. Allegri, A. Colpani, P. S. Ginestra, and A. Attanasio, "An experimental study on micro-milling of a medical grade Co-Cr-Mo alloy produced by selective laser melting," *Materials (Basel).*, vol. 12, no. 13, 2019, doi: 10.3390/ma12132208.

[3] M. Vignesh *et al.*, "Development of Biomedical Implants through Additive Manufacturing: A Review," *J. Mater. Eng. Perform.*, vol. 30, no. 7, pp. 4735–4744, 2021, doi: 10.1007/s11665-021-05578-7.

[4] H. Salem, L. N. Carter, M. M. Attallah, and H. G. Salem, "Influence of processing parameters on internal porosity and types of defects formed in Ti6Al4V lattice structure fabricated by selective laser melting," *Mater. Sci. Eng. A*, vol. 767, no. May, p. 138387, 2019, doi: 10.1016/j.msea.2019.138387.

[5] S. K. Gupta *et al.*, "Enhanced biomechanical performance of additively manufactured Ti-6Al-4V bone plates," *J. Mech. Behav. Biomed. Mater.*, vol. 119, no. March, p. 104552, 2021, doi: 10.1016/j.jmbbm.2021.104552.

[6] P. Ginestra *et al.*, "Post processing of 3D printed metal scaffolds: A preliminary study of antimicrobial efficiency," *Procedia Manuf.*, vol. 47, no. 2019, pp. 1106–1112, 2020, doi: 10.1016/j.promfg.2020.04.126.

[7] L. Riva, P. S. Ginestra, and E. Ceretti, "Mechanical characterization and properties of laser-based powder bed–fused lattice structures: a review," *Int. J. Adv. Manuf. Technol.*, vol. 113, no. 3–4, pp. 649–671, 2021, doi: 10.1007/s00170-021-06631-4.

[8] P. Ginestra *et al.*, "Surface ace finish of A Additi dditiv vel ely y Manuf Manufactur actured ed Metals : biofilm f formation ormation and cellular attachment 1 Intr Introduction oduction 2 Manuf Manufacturing acturing and post pr processing ocessing treatment," vol. 13, pp. 1–12, 2021.

[9] T. Majumdar, T. Bazin, E. M. C. Ribeiro, J. E. Frith, and N. Birbilis, "Understanding the effects of PBF process parameter interplay on Ti-6Al-4V surface properties," *PLoS One*, vol. 14, no. 8, pp. 1–24, 2019, doi: 10.1371/journal.pone.0221198.

[10] M. Nakatani, H. Masuo, Y. Tanaka, and Y. Murakami, "Effect of Surface Roughness on Fatigue Strength of Ti-6Al-4V Alloy Manufactured by Additive Manufacturing," *Procedia Struct. Integr.*, vol. 19, pp. 294–301, 2019, doi: 10.1016/j.prostr.2019.12.032.